Materials Advances

ROYAL SOCIETY OF CHEMISTRY

PAPER

View Article Online
View Journal

Cite this: DOI: 10.1039/d5ma00743g

Ultrathin millimeter-wave–absorbing film for automotive radars based on an epsilon iron oxide/carbon nanotube composite material

Asuka Namai, *[a] Marie Yoshikiyo, [a] Jessica MacDougall, [a] Takashi Ono,[b] Takahiro Asai,[b] Masayuki Hara,[b] Momoe Kanai,[b] Takayuki Yoshida,[c] Yasuto Miyamoto,[c] Kenji Sakane,[c] Shinji Kurahashi,[d] Toshifumi Nishio[d] and Shin-ichi Ohkoshi *[ae]

Received 12th July 2025,
Accepted 28th October 2025

DOI: 10.1039/d5ma00743g

rsc.li/materials-advances

Millimeter waves are used in automotive radars to detect surrounding objects such as vehicles and pedestrians. In millimeter-wave automotive radar systems, unnecessary millimeter waves arising from the radar system itself and other radar sources should be suppressed. Herein, we report an ultrathin millimeter-wave–absorbing film for the automotive radar frequency band (79 GHz) based on a composite of gallium-substituted epsilon iron oxide (ε-$Ga_{0.45}Fe_{1.55}O_3$) nanomagnets, which exhibit a high magnetic permeability, and carbon nanotubes (CNTs), which exhibit a high dielectric constant. The composite exhibits a complex dielectric constant ($\varepsilon = \varepsilon' - i\varepsilon''$) of ε' = 19.4 and ε'' = 3.3 and a complex magnetic permeability ($\mu = \mu' - i\mu''$) of μ' = 0.87 and μ'' = 0.13 at 79 GHz. Using this composite, we prepared an ultrathin millimeter-wave–absorbing film which shows a reflection loss of −21.4 dB (99.3% suppression) at 79 GHz with a thickness of 213 ± 8 μm. This ultrathin millimeter-wave–absorbing film can be easily coated on radar device covers, automotive parts such as bumpers, and infrastructure components like guardrails and traffic lights.

Introduction

Millimeter-wave radars have become important devices for autonomous driving.[1,2] Millimeter-wave radars using the 79 GHz band are widely used in automotive collision avoidance systems to detect surrounding objects such as automobiles, motorbikes, bicycles, and pedestrians. Effective use of millimeter-wave radars requires suppressing noise arising from the radar system itself and other radar sources, as these noises may cause detection errors and reduce sensitivity. Therefore, developing millimeter-wave absorbers is important.[3,4] Thin and flexible films and ink are especially desirable for millimeter-wave absorption, as they enable application to radar covers, automotive components such as bumpers, and infrastructure such as guardrails and traffic lights.

To absorb electromagnetic waves, there are mainly two mechanisms: magnetic loss due to high magnetic permeability and dielectric loss due to high dielectric constant.[5,6] This study aims to develop a millimeter-wave–absorbing thin film that combines both a high magnetic permeability and a high dielectric constant. For a high magnetic permeability in the millimeter-wave region, we focus on epsilon iron oxide (ε-Fe_2O_3),[7,8] which shows millimeter-wave absorption *via* magnetic loss from zero-field ferromagnetic resonance at 182 GHz.[9–11] Such a high resonance frequency arises from the strong magnetocrystalline anisotropy of ε-Fe_2O_3,[12–22] and the resonance frequency of ε-Fe_2O_3 can be tuned across a wide range from 35 GHz to 222 GHz, by substituting Fe^{3+} with the other metal cations such as Al^{3+}, Ti^{4+}–Co^{2+}, Mn^{2+}, Ga^{3+}, In^{3+}, Rh^{3+}, or combinations of them.[23–31] The strategy of the present work to achieve a high dielectric constant in the millimeter-wave region is to develop a pseudo-dielectric material by combining an electrically conductive material and an insulating material. In this study, carbon nanotubes (CNTs) were selected as the electrically conductive material, due to their high electrical conductivity.[32–34] Herein, we report an ultrathin millimeter-wave–absorbing film based on a composite of gallium-substituted ε-Fe_2O_3 (ε-$Ga_xFe_{2-x}O_3$) nanomagnets and CNTs.

[a] Department of Chemistry, School of Science, The University of Tokyo, 7-3-1 Hongo, Bunkyo-ku, Tokyo 113-0033, Japan. E-mail: asuka@chem.s.u-tokyo.ac.jp, ohkoshi@chem.s.u-tokyo.ac.jp
[b] Tokyo Ohka Kogyo Co., Ltd, 1590 Tabata, Samukawa-machi, Koza-gun, Kanagawa 253-0114, Japan
[c] Dowa Electronics Materials Co., Ltd., 1-3-1 Kaigandori, Minami-ku, Okayama 702-8506, Japan
[d] Ehime Institute of Industrial Technology, 487-2, Kubota-cho, Kurume, Matsuyama city, Ehime 791-1101, Japan
[e] CNRS International Research Laboratory DYNACOM, 7-3-1 Hongo, Bunkyo-ku, Tokyo 113-0033, Japan

Results and discussion

High magnetic permeability of ε-$Ga_{0.45}Fe_{1.55}O_3$ nanomagnets

To adjust the zero-field ferromagnetic resonance frequency of ε-Fe_2O_3 nanomagnets to the millimeter-wave radar frequency, ε-$Ga_{0.45}Fe_{1.55}O_3$ nanomagnets were employed (Fig. S1). ε-$Ga_{0.45}Fe_{1.55}O_3$ nanomagnets were synthesized by the sol–gel method following a previous report.[26] The details are provided in the Experimental section of the SI. Inductively coupled plasma atomic emission spectrometry (ICP-AES) measurement indicated that the formula of the obtained sample is $Ga_{0.45}Fe_{1.55}O_3$. Calcd: Fe, 52.14%; Ga, 18.93%; Found: Fe, 52.07%; Ga, 18.91%. Transmission electron microscopy (TEM) images showed that the sample was composed of nanoparticles with a size of 27 ± 9 nm (Fig. 1a). The powder X-ray diffraction (PXRD) pattern with Rietveld analysis indicated that the sample is composed of pure ε-$Ga_{0.45}Fe_{1.55}O_3$ (orthorhombic, $Pna2_1$ space group, a = 5.08793(10), b = 8.7736(2), c = 9.4375(2), and V = 421.289(13)) (Fig. S2 and Table S1). The magnetic properties were measured using a superconductive quantum interference device (SQUID). ε-$Ga_{0.45}Fe_{1.55}O_3$ exhibits hard magnetic behavior at 300 K, with a coercive field (H_c) of 7.3 kOe, saturation magnetization of 26.2 emu g^{-1} at 5 T, and remanent magnetization of 12.3 emu g^{-1} (Fig. 1b).

To evaluate the complex magnetic permeability ($\mu = \mu' - i\mu''$), the millimeter-wave absorption spectrum was measured using a terahertz time-domain spectroscopy (THz-TDS) system. Fig. 1c shows the diagram of the measurement system. A THz pulse was irradiated onto the sample and the transmitted THz pulse was detected in the time domain, and then Fourier transformed into an absorption spectrum in the frequency domain. For this measurement, powder-form ε-$Ga_{0.45}Fe_{1.55}O_3$ was compressed into a pellet with a diameter of 13 mmϕ, a thickness of 2.60 mm, and a filling ratio of 55 vol%. In the absorption spectrum, a peak due to zero-field ferromagnetic resonance was observed at 77 GHz (Fig. S3). The μ and ε values were evaluated by analyzing the absorption spectrum, assuming that μ obeys the Landau-Lifshitz equation,[35] and ε is a constant value (SI, section §4). Fig. 1d shows the frequency dependence of μ' and μ''. As the frequency increased, μ' initially reached a maximum of μ'_{max} = 1.52 at 75 GHz, then decreased to μ' = 1 at the resonance frequency of 77 GHz, continued to decrease to a minimum of μ'_{min} = 0.48 at 79 GHz, and gradually recovered approaching 1 (Fig. 1d, left). Meanwhile, μ'' showed a peak at the resonance frequency of 77 GHz, with a maximum value of μ''_{max} = 1.03 (Fig. 1d, right). As for the complex dielectric constant ($\varepsilon = \varepsilon' - i\varepsilon''$), the ε' and ε'' values were 11.1 and 0.42, respectively (Fig. S4).

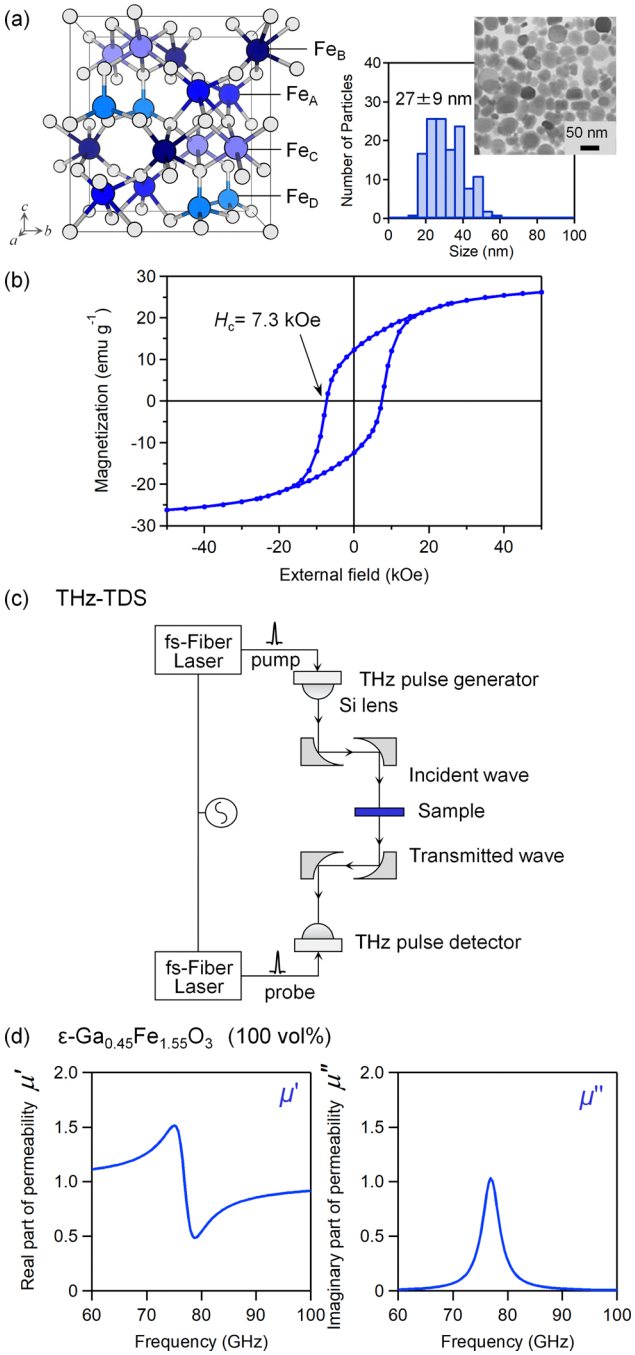

Fig. 1 (a) Crystal structure, TEM image, particle size distribution of ε-$Ga_{0.45}Fe_{1.55}O_3$ nanomagnets. (b) Magnetization *versus* external magnetic field curve of ε-$Ga_{0.45}Fe_{1.55}O_3$ measured at 300 K. (c) Diagram of the THz-TDS system. (d) Frequency dependence of μ' and μ'' for ε-$Ga_{0.45}Fe_{1.55}O_3$ nanomagnets, calibrated by the filling ratio.

High dielectric constant of CNTs in resin

To prepare a high dielectric composite material in the millimeter-wave region, multiwalled-CNTs (VGCF-H, Resonac Holdings Corporation) were used as the electrically conductive material. TEM and scanning electron microscopy (SEM) images show that the CNTs have an average length of 2 ± 1 μm and a diameter of 130 ± 60 nm (Fig. 2 and Fig. S5).

To obtain a high dielectric constant material, CNTs were dispersed in a cellulose resin as follows. A cellulose resin was first dissolved in terpineol, and then CNTs were dispersed in the solution by homogenization. The resulting suspension was cast and dried to obtain sheets with CNT concentrations of 0, 5, 6, and 8 vol%. The complex dielectric constant in the millimeter-wave region was evaluated by THz-TDS. The absorption spectra were analyzed assuming μ = 1 for non-magnetic

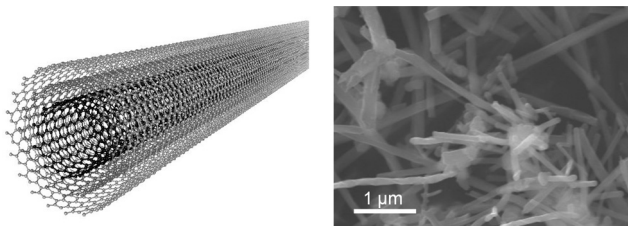

Fig. 2 Schematic illustration (left) and SEM image (right) of CNTs.

materials. Fig. 3 shows the frequency dependence of ε' and ε'' values of the sheet containing 5 vol% CNTs. Both the ε' and ε'' values were high, *e.g.*, $(\varepsilon', \varepsilon'') = (13.7, 2.5)$ at 79 GHz. Increasing the CNT concentration increased the ε values, *e.g.*, $(\varepsilon', \varepsilon'') = (20.1, 3.7)$ for 6 vol% CNTs, and $(22.1, 5.0)$ for 8 vol% CNTs at 79 GHz (Fig. S6). The observed high dielectric constants in the millimeter wave region were analyzed based on the Maxwell–Wagner–Sillars (MWS) model using the following equation,[36–39]

$$\varepsilon(f) = \varepsilon_\infty + \frac{\Delta\varepsilon}{1+(2i\pi\tau f)^{1-\alpha}} - \frac{i\sigma_{dc}}{2\pi\varepsilon_0 f}$$

where ε_∞ is the real part of the dielectric constant at $f \to \infty$, $\Delta\varepsilon$ is the difference between the static dielectric constant ε_s at $f = 0$ and ε_∞ ($\Delta\varepsilon = \varepsilon_s - \varepsilon_\infty$), α is the stretching exponent for the Cole–Cole element, τ is the median MWS relaxation time, σ_{dc} is the dc conductivity, ε_0 is the permittivity of vacuum, and i is the imaginary unit. The fitting results showed that both $\Delta\varepsilon$ and σ_{dc} increased with increasing CNT concentration, indicating enhancements in both dielectric and conductive losses (Fig. S7, S8 and Table S2). The high $\Delta\varepsilon$ values suggest that the conductive CNTs dispersed in the insulating cellulose resin behave as a pseudo-dielectric material. This behavior can be explained as follows: when millimeter waves are irradiated onto the conductive CNTs dispersed within the cellulose matrix, the electric field of the waves induces electron flow. These electrons are scattered at the interfaces between the CNTs and the surrounding resin, resulting in dissipation of electromagnetic wave energy. Furthermore, as the CNT concentration increases, percolation among CNTs progresses, resulting in an increase in conductive loss. Consequently, high ε' and ε'' values are achieved in the millimeter-wave region.

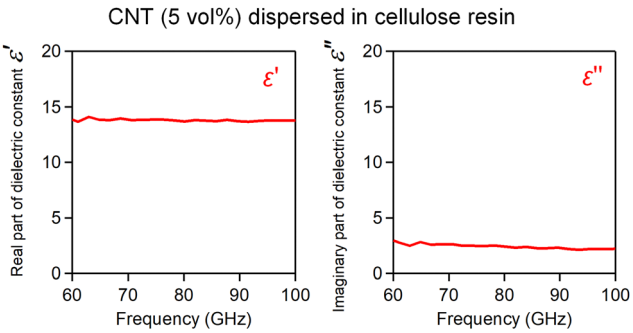

Fig. 3 Frequency dependence of ε' and ε'' for CNTs dispersed in cellulose resin with a concentration of 5 vol%.

High magnetic permeability and high dielectric constant of a composite of ε-$Ga_{0.45}Fe_{1.55}O_3$ nanomagnets and CNTs

Next, we prepared a composite of ε-$Ga_{0.45}Fe_{1.55}O_3$ nanomagnets and CNTs with a volume ratio of ε-$Ga_{0.45}Fe_{1.55}O_3$: CNT : cellulose resin = 35 : 5 : 60. SEM images of the composite are shown in Fig. S9. The ε and μ values were evaluated by THz-TDS using a sheet-form sample with a thickness of 545 μm (Fig. S10). As shown in Fig. 4a, the composite exhibits a high ε value of $(\varepsilon', \varepsilon'') = (19.4, 3.3)$. The composite also exhibits a high μ value, where the μ'_{max} and μ'_{min} values are 1.13 and 0.87, respectively, μ''_{max} is 0.26, and FWHM is 3.8 GHz (Fig. 4b). Both ε'' and μ'' contribute to dissipation of the electromagnetic wave energy.

Design of ultrathin millimeter-wave–absorbing film

Next, we designed an ultrathin millimeter-wave–absorbing film. To achieve high absorption performance with a thin film, the impedance-matching technique is effective. Here, we consider an absorber attached to a metal plate (Fig. 5a). When a millimeter wave is irradiated to the absorber, part of the millimeter wave is reflected at the surface of the absorber, while the remainder penetrates the absorber and is reflected at the metal surface. If these two reflected waves compensate each other in opposite phases, the millimeter-wave absorption is enhanced. The condition is described as $d = \lambda_{absorber}/4 = \lambda_{incident}/4\sqrt{\varepsilon\mu}$, where d is the absorber thickness, $\lambda_{incident}$ is the wavelength of the incident millimeter wave, $\lambda_{absorber}$ is the wavelength of the millimeter wave inside the absorber, and ε and μ are the complex dielectric constant and complex magnetic permeability of the absorber,

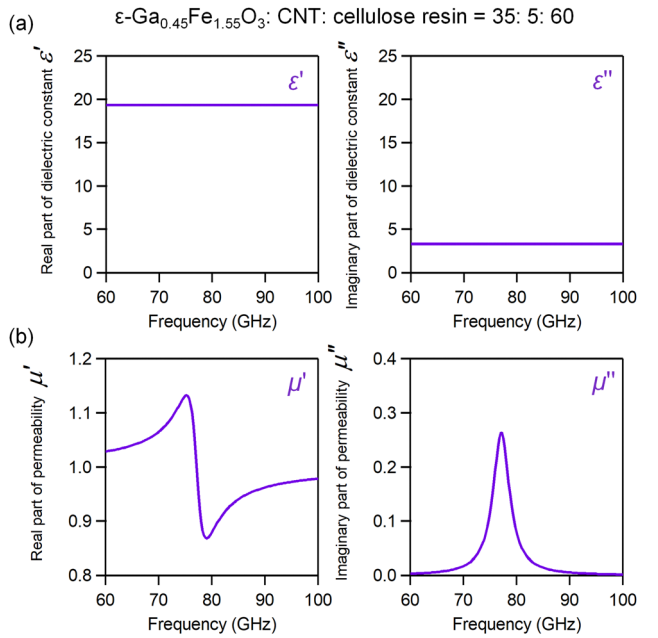

Fig. 4 Frequency dependence of (a) ε' and ε'', (b) μ' and μ'' for the composite (ε-$Ga_{0.45}Fe_{1.55}O_3$: CNT : cellulose resin = 35 : 5 : 60) evaluated from the absorption spectrum of the sheet-form sample.

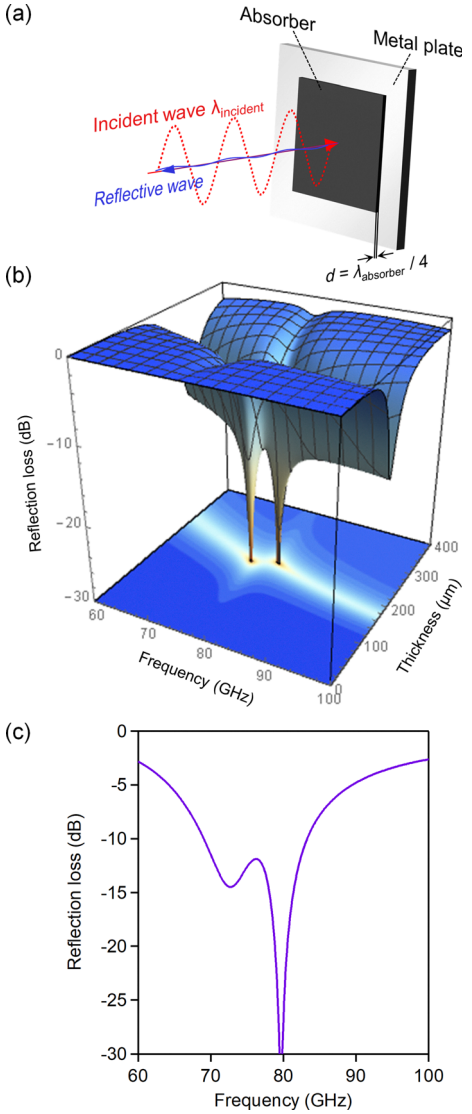

Fig. 5 (a) Schematic illustration of an absorber attached on a metal plate. (b) Three-dimensional map of the simulated *RL* value for the composite with respect to the thickness *d* and frequency *f*. (c) Frequency dependence of the *RL* value for an absorber with a thickness of 231 μm, which is an impedance matching condition at 79 GHz.

respectively. Reflection loss (*RL*) is calculated based on transmission theory, using the following equations.[40–42]

$$RL[\mathrm{dB}] = 20\log_{10}\left|\frac{Z-1}{Z+1}\right|$$

$$Z = \frac{\sqrt{\mu}}{\sqrt{\varepsilon}}\tanh\left(i\frac{2\pi fd}{c}\sqrt{\mu\cdot\varepsilon}\right)$$

where Z is a normalized input impedance, f is the frequency of the incident wave, c is the speed of the light, and i is the imaginary unit.

Fig. 5b shows a three-dimensional map of the simulated *RL* value for the composite as a function of the thickness d and frequency f. The two *RL* minima are around the resonance frequency, which are due to the frequency dependence of μ of

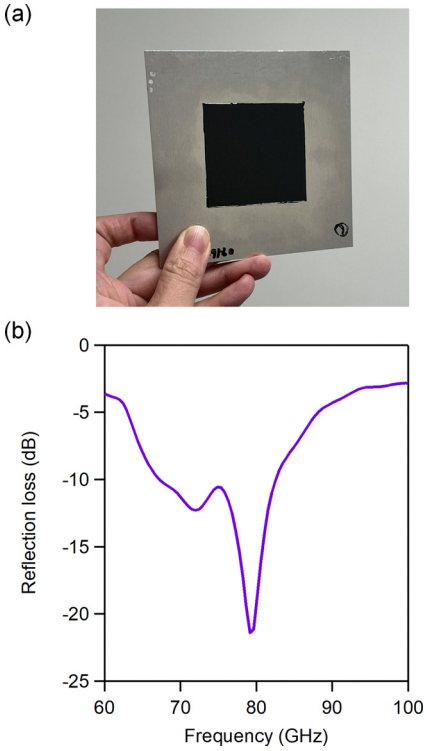

Fig. 6 (a) Photograph of the fabricated millimeter-wave–absorbing film on a metal plate. (b) Observed *RL* spectrum of the film.

ε-$Ga_{0.45}Fe_{1.55}O_3$. As shown in Fig. 5c, a strong absorption at 79 GHz is expected by impedance matching.

Based on the simulation, we prepared a thin composite film on a metal plate (Fig. 6a). The thickness was evaluated with a stylus step gauge as 213 ± 8 μm. The *RL* spectrum of the metal-backed film showed a minimum at 79 GHz with *RL* = −21.4 dB, corresponding to 99.3% absorption (Fig. 6b). The bandwidth at *RL* = −10 dB (90% absorption) was as wide as 15.3 GHz. As for millimeter-wave absorbing materials in similar frequency region, several absorbers have been reported in addition to ε-iron-oxide–based absorbers, *e.g.*, TiO_2/carbon/resin (350 μm thick), permalloy/chlorinated polyethylene/binder (1.4 mm thick), Al_2O_3/carbon black/resin (1.1 mm thick), and carbonyl iron/CNT/resin (2.9 mm thick) composites.[28,31,43–46] In these absorbers, the absorption properties originate solely from dielectric loss (including conductive loss). In contrast, the absorber developed in this study utilizes both magnetic loss arising from ε-$Ga_{0.45}Fe_{1.55}O_3$ and dielectric loss originating from CNTs, enabling the realization of a thin absorber with high performance.

Conclusion

In this study, we prepared an ultrathin millimeter-wave absorber composed of ε-$Ga_{0.45}Fe_{1.55}O_3$ nanomagnets and CNTs dispersed in cellulose resin exhibiting both high magnetic permeability and high dielectric constant. The composite exhibited a complex dielectric constant of $(\varepsilon', \varepsilon'')$ = (19.4, 3.3) and a complex magnetic permeability (μ', μ'') = (0.87, 0.13) at 79 GHz. By employing the

impedance-matching technique, a strong reflection loss of −21.4 dB (99.3% absorption) was achieved at the automotive radar frequency of 79 GHz. We have confirmed that the present absorber is stable even after 10 years. The solution-based coating process also allows easy application onto various metal surfaces with curved or complex structures, *e.g.*, radar device covers, automotive parts such as bumpers, and infrastructure components such as guardrails and traffic lights. Moreover, by adjusting the composition of the metal-substituted ε-Fe_2O_3, the absorption frequency can be tuned for further applications such as sixth-generation wireless communication networks (6G).[47–51] Other conductive materials such as MXenes,[39] as well as high dielectric materials such as graphene oxide,[52] are also considered promising for combination with metal-substituted ε-Fe_2O_3 to achieve thin, high-performance millimeter wave absorbers.

Conflicts of interest

There are no conflicts to declare.

Data availability

Data supporting this article has been included as part of the supplementary information (SI). Supplementary information is available. See DOI: **https://doi.org/10.1039/d5ma00743g**.

Acknowledgements

This work was supported in part by a Grant-in-Aid for Scientific Research A from the Japan Society for the Promotion of Science (JSPS) (Grant Number 25H00866), a Grant-in-Aid for Scientific Research B from JSPS (Grant Numbers 23H01920), a Grant-in-Aid for Young Scientists from JSPS (Grant number JP24K17606). We recognize the Cryogenic Research Center at The University of Tokyo, DOWA Technofund, the Tokyo Ohka Foundation for The Promotion of Science and Technology, and the Center for Nano Lithography & Analysis at The University of Tokyo.

Notes and references

1 S. Patole, M. Torlak, D. Wang and M. Ali, *IEEE Signal Process. Mag.*, 2017, **34**, 22–35.
2 J. Choi, V. Va, N. González-Prelcic, R. Daniels, C. R. Bhat and R. W. Heath, *IEEE Commun. Mag.*, 2016, **54**, 160–167.
3 N. K. Narayanaswamy, T. Y. Satheesha, Y. Alzahrani, A. Pandey, A. K. Dwivedi, V. Singh and M. Tolani, *Sci. Rep.*, 2024, **14**, 30199.
4 M. Al-Hasan, I. Ben Mabrouk, E. R. F. Almajali, M. Nedil and T. A. Denidni, *IEEE Access*, 2019, **7**, 58466–58474.
5 Y. Kotsuka, *Electromagnetic wave absorbers: detailed theories and applications*, John Wiley & Sons, Inc, Hoboken, New Jersey, 2019.
6 H. Wu, J. Luo and M. Yang, *Electromagnetic wave absorbing materials: fundamentals and applications*, Wiley, Hoboken, New Jersey, 2024.
7 J. Jin, S. Ohkoshi and K. Hashimoto, *Adv. Mater.*, 2004, **16**, 48–51.
8 J. Tucek, R. Zboril, A. Namai and S. Ohkoshi, *Chem. Mater.*, 2010, **22**, 6483–6505.
9 S. Ohkoshi, A. Namai, T. Yamaoka, M. Yoshikiyo, K. Imoto, T. Nasu, S. Anan, Y. Umeta, K. Nakagawa and H. Tokoro, *Sci. Rep.*, 2016, **6**, 27212.
10 E. Gorbachev, M. Soshnikov, M. X. Wu, L. Alyabyeva, D. Myakishev, E. Kozlyakova, V. Lebedev, E. Anokhin, B. Gorshunov, O. Brylev, P. Kazin and L. Trusov, *J. Mater. Chem. C*, 2021, **9**, 6173–6179.
11 S. Ohkoshi, M. Yoshikiyo, K. Imoto, K. Nakagawa, A. Namai, H. Tokoro, Y. Yahagi, K. Takeuchi, F. D. Jia, S. Miyashita, M. Nakajima, H. S. Qiu, K. Kato, T. Yamaoka, M. Shirata, K. Naoi, K. Yagishita and H. Doshita, *Adv. Mater.*, 2020, **32**, 2004897.
12 Y.-C. Tseng, N. M. Souza-Neto, D. Haskel, M. Gich, C. Frontera, A. Roig, M. van Veenendaal and J. Nogués, *Phys. Rev. B: Condens. Matter Mater. Phys.*, 2009, **79**, 094404.
13 S. Ohkoshi, A. Namai, K. Imoto, M. Yoshikiyo, W. Tarora, K. Nakagawa, M. Komine, Y. Miyamoto, T. Nasu, S. Oka and H. Tokoro, *Sci. Rep.*, 2015, **5**, 14414.
14 S. Ohkoshi, A. Namai, M. Yoshikiyo, K. Imoto, K. Tamazaki, K. Matsuno, O. Inoue, T. Ide, K. Masada, M. Goto, T. Goto, T. Yoshida and T. Miyazaki, *Angew. Chem., Int. Ed.*, 2016, **55**, 11403–11406.
15 J. L. García-Muñoz, A. Romaguera, F. Fauth, J. Nogués and M. Gich, *Chem. Mater.*, 2017, **29**, 9705–9713.
16 S. Ohkoshi, K. Imoto, A. Namai, S. Anan, M. Yoshikiyo and H. Tokoro, *J. Am. Chem. Soc.*, 2017, **139**, 13268–13271.
17 K. T. Chan, J. R. Morales, Y. Kodera and J. E. Garay, *J. Mater. Chem. C*, 2017, **5**, 7911–7918.
18 I. Ahamed, R. Pathak, R. Skomski and A. Kashyap, *AIP Adv.*, 2018, **8**, 055815.
19 S. Ohkoshi, K. Imoto, A. Namai, M. Yoshikiyo, S. Miyashita, H. S. Qiu, S. Kimoto, K. Kato and M. Nakajima, *J. Am. Chem. Soc.*, 2019, **141**, 1775–1780.
20 J. Yuan, A. Balk, H. Guo, Q. Fang, S. Patel, X. Zhao, T. Terlier, D. Natelson, S. Crooker and J. Lou, *Nano Lett.*, 2019, **19**, 3777–3781.
21 Y. Z. Wang, P. Wang, H. Wang, B. Q. Xu, H. Li, M. Cheng, W. Feng, R. F. Du, L. Y. Song, X. Wen, X. H. Li, J. B. Yang, Y. Cai, J. He, Z. X. Wang and J. P. Shi, *Adv. Mater.*, 2023, **35**, 2209465.
22 W. H. Xue, T. Wang, H. L. Yang, H. H. Zhang, G. H. Dai, S. Zhang, R. L. Yang, Z. Y. Quan, R. W. Li, J. Tang, C. Song and X. H. Xu, *Nat. Commun.*, 2025, **16**, 440.
23 A. Namai, S. Sakurai, M. Nakajima, T. Suemoto, K. Matsumoto, M. Goto, S. Sasaki and S. Ohkoshi, *J. Am. Chem. Soc.*, 2009, **131**, 1170–1173.
24 A. Namai, K. Ogata, M. Yoshikiyo and S. Ohkoshi, *Bull. Chem. Soc. Jpn.*, 2020, **93**, 20–25.
25 J. MacDougall, A. Namai, O. Strolka and S. Ohkoshi, *Mater. Adv.*, 2025, **6**, 969–976.
26 S. Ohkoshi, S. Kuroki, S. Sakurai, K. Matsumoto, K. Sato and S. Sasaki, *Angew. Chem., Int. Ed.*, 2007, **46**, 8392–8395.

27 G. R. Jo, M. B. Yun, Y. H. Son, B. Park, J. G. Lee, Y. G. Kim, Y. G. Son and Y. K. Baek, *Chem. Commun.*, 2022, **58**, 11442–11445.
28 L. Wan and X. Xu, *Appl. Phys. A: Mater. Sci. Process.*, 2024, **130**, 925.
29 M. Yoshikiyo, A. Namai, M. Nakajima, K. Yamaguchi, T. Suemoto and S. Ohkoshi, *J. Appl. Phys.*, 2014, **115**, 172613.
30 A. Namai, M. Yoshikiyo, K. Yamada, S. Sakurai, T. Goto, T. Yoshida, T. Miyazaki, M. Nakajima, T. Suemoto, H. Tokoro and S. Ohkoshi, *Nat. Commun.*, 2012, **3**, 1035.
31 R. Kinugawa, K. Imoto, Y. Futakawa, S. Shimizu, R. Fujiwara, M. Yoshikiyo, A. Namai and S. Ohkoshi, *Adv. Eng. Mater.*, 2021, **23**, 2001473.
32 M. F. L. De Volder, S. H. Tawfick, R. H. Baughman and A. J. Hart, *Science*, 2013, **339**, 535–539.
33 I. I. Nefedova, D. V. Lioubtchenko, I. S. Nefedov and A. V. Räisänen, *IEEE Trans. Microwave Theory Tech.*, 2015, **63**, 3265–3271.
34 H. P. Fu, C. Yang, K. X. Ma, H. Huang, J. G. Ma, Y. L. Li, Y. R. Kang, J. X. Ma and X. D. Huang, *AIP Adv.*, 2018, **8**, 085110.
35 L. Landau and E. Lifshitz, *Phys. Z. Sowjetunion*, 1935, **8**, 153–169.
36 J. C. Maxwell, *A Treatise on Electricity and Magnetism*, Dover Publications, Wales, 1954.
37 X. D. Xia, Z. Zhong and G. J. Weng, *Mechnol. Mater.*, 2017, **109**, 42–50.
38 Z. Q. Guo, J. W. Ren, X. Z. Xu, D. Lan, S. Y. Zhang, M. K. He, Z. G. Gao, Z. R. Jia and G. L. Wu, *J. Mater. Sci. Technol.*, 2025, **236**, 19–27.
39 S. Zhang, M. R. Li, G. N. Chen, H. L. Wang, G. Shao, D. Lan, Y. Q. Zhu, R. Zhang, L. Guan and B. B. Fan, *J. Alloys Compd.*, 2025, **1023**, 180015.
40 M. Qin, L. Zhang and H. Wu, *Adv. Sci.*, 2022, **9**, 2105553.
41 X. Zeng, X. Cheng, R. Yu and G. D. Stucky, *Carbon*, 2020, **168**, 606–623.
42 S. S. Kim, S. B. Jo, K. I. Gueon, K. K. Choi, J. M. Kim and K. S. Churn, *IEEE Trans. Magn.*, 1991, **27**, 5462–5464.
43 T. Soh and O. Hashimoto, *Electron. Commun. Jpn.*, 2003, **86**, 52–58.
44 C. M. Choi, D. I. Kim, S. H. Je and Y. S. Choi, *Curr. Appl. Phys.*, 2007, **7**, 586–589.
45 Y. Takase, O. Hashimoto, K. Matsumoto and T. Kumada, *Electron. Commun. Jpn.*, 2010, **93**, 25–33.
46 Y. R. Wang, R. Y. Su, J. Y. Chen, W. Q. Wang, X. Q. Zhang, H. Xu and R. J. He, *ACS Appl. Mater. Interfaces*, 2023, **15**, 53996–54005.
47 J. Ma, R. Shrestha, J. Adelberg, C. Y. Yeh, Z. Hossain, E. Knightly, J. M. Jornet and D. M. Mittleman, *Nature*, 2018, **563**, 89–93.
48 S. Koenig, D. Lopez-Diaz, J. Antes, F. Boes, R. Henneberger, A. Leuther, A. Tessmann, R. Schmogrow, D. Hillerkuss, R. Palmer, T. Zwick, C. Koos, W. Freude, O. Ambacher, J. Leuthold and I. Kallfass, *Nat. Photon.*, 2013, **7**, 977–981.
49 Y. Yan, G. Xie, M. P. Lavery, H. Huang, N. Ahmed, C. Bao, Y. Ren, Y. Cao, L. Li, Z. Zhao, A. F. Molisch, M. Tur, M. J. Padgett and A. E. Willner, *Nat. Commun.*, 2014, **5**, 4876.
50 S. Rangan, T. S. Rappaport and E. Erkip, *Proc. IEEE*, 2014, **102**, 366–385.
51 A. Kumar, M. Gupta and R. Singh, *Nat. Electron.*, 2022, **5**, 261–262.
52 A. Romanowska, S. Marynowicz, T. Strachowski, K. Godziszewski, Y. Yashchyshyn, A. Racki, M. Baran, T. Ciuk and A. Chlanda, *IEEE Trans. Nanotechnol.*, 2024, **23**, 329–337.